How will technology facilitate Agile Discovery?

James S Cleverley
Global Product Manager – Geosciences, Imdex Limited, Iford, East Sussex, UK

Abstract. The process of Ore Discovery, and the delivery of a reportable resource, is often driven by waterfall processes. Each step in the process is sequential, with long delays waiting for data and information to decide on the best action. In many cases the decision about what to do next is made long after the drilling or sampling program has finished, or, without reliable information to support the decision. Cleverley et al. (2017) discussed the impact on the minerals discovery process of decreasing the time spent within the drilling cycle, from changing the technology of drilling to managing data workflows, to changes in behaviour and systems. The technology now exists that can be used to change the drilling to decision paradigm, but are we ready as an industry to adapt to this change? What is the impact of technology adoption on our ability to act on a quicker decision – business systems, people and regulatory process. Implementing technology is just the start of the change we need to address in order to achieve the potential value that new technology will unlock.

1 Waterfall or Agile?

In the business world, especially prevalent in technology start-ups in the last 15 years, there has been a shift from traditional waterfall project management to Agile processes. The Agile manifesto was a set of four values developed in 2001 (https://agilemanifesto.org/) that provided a framework for software development moving from rigid, onerous, pre-determined plans to value feedback, and dynamic learning as part of the development process. This approach is more recently finding its way into other product development disciplines. The key driver behind the agile approach to projects is not to operate in chaos, but to follow a roadmap with the ability to test, learn and revise as you go.

Figure 1 compares the timeline of a project delivered by waterfall process versus an agile framework. In the latter the project is continually evolved, and each iteration delivers a refinement of understanding, reducing risk and informing the next iteration. In the waterfall process the planning becomes critical and there is little room to change the direction or intent half way through without restarting the whole process. This same process can be applied to the way we discover resources, or plan to mine them. Replace the software release with a resource update. The long and comprehensive waterfall approach will deliver a high-quality resource at the end but the time to deliver is long and is not influenced by testing the model along the way. The resource update is comprehensive but high risk in that it is still dependant on the very first data. In the alternative approach an exploration project will deliver incremental resource updates along the way. These will be fast, lower resolution, less complete but will inform what is done next to reduce risk, improve resources or even walk away early. At each step the program will be optimised to maximise information entropy. The ultimate reported resource is higher quality with more confidence because we have taken risk away throughout the process – this de-risking requires informed geoscience thinking where it's needed along the way, but it also requires lots of feedback built on rapidly delivered geoscience data and analysis.

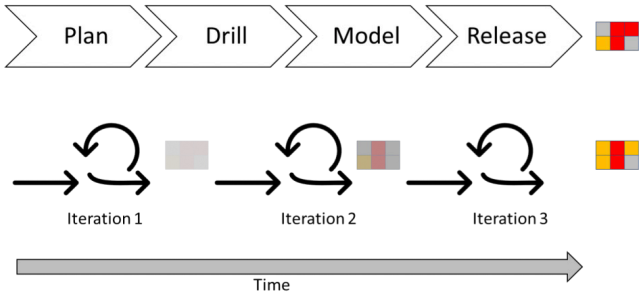

Figure 1. The comparison between Waterfall (top) and Agile (bottom) project processes over time. While the Waterfall processes deliver a high-quality model there is no risk reduction with incremental learnings, where Agile processes deliver iterative models with progressively increasing confidence. The iterative process allows for testing and learning along the program path.

2 How can Agile Exploration be delivered?

Operating a project in an Agile framework values the understanding over the process, allowing rapid iterations in order to refine your model. In software development this is about quickly testing your understanding of what the customer wants with releases. Refining the learnings about the customer allows the project to circle back and try something new – the feature release.

In the process of minerals discovery or resource definition it is harder to conceptualise being able to rapidly iterate our understanding. The length of time taken to plan, execute, interpret and make a decision is typically on the scale of weeks or months, certainly in many cases longer than a single campaign. However, the last few years as seen the introduction of new connected sensing technology that can provide near real-time data during drilling and sampling. This allows for a different approach to exploration programs, one that is built on the ability to make a decision in near real-time.

For example, Noble et al. (2018) demonstrated the use of in-field sample preparation and analysis with portable XRF to dynamically manage a Helicopter soil sampling program in South Australia. Samples could be collected and delivered to camp, prepared and analysed, and the sampling plan modified for day 2 or 3 on the results from

day 1. This allows for real-time follow up of anomalies and less wasted analyses of “dead” zones. The samples are still analysed at a commercial laboratory for high quality, low detection limit data, but the decision about which samples to take, and the impact on the sampling program (change, move on, infill) can be made at the time of mobilisation. There are similar examples of technology being used in the process of drilling, either downhole or top of analysis, that can be used to drive the decision process around a program.

It is not just the process of delivering near real-time data from sensors that allows for decisions to be made. Data needs to be managed, securely transmitted and presented to the geoscientist in a way that allows information to support the decision. This might be at the drill rig or field camp, but equally could be back at head office or as a collaboration across multiple functions anywhere in the globe. This ability to provide connected data through cloud infrastructure is something that we take for granted in consumer products (step trackers, google maps traffic), but is new for the minerals industry. IMDEXHUB-IQ™ is an example of web

3 What are the challenges to adoption?

The minerals industry is facing a world where IoT connected sensing devices will allow the delivery of geoscience data from the drill rig or sampling program to the decision maker. This data will need to be analysed in a timely manner using analytics to support the interpretation, but critically requiring good, quantitative, numerical geoscience. In an Agile Exploration framework, the workflows of people are impacted, with more emphasis on using the data to decide in a time frame that adds value. As highlighted in Cleverley et al. (2017) there are barriers to adoption of technology not driven by whether the technology itself works, but by understanding how to implement all of the workflows and processes around the new Agile paradigm to realise the maximum value. These include business systems, data systems and security, workflow of people, remote collaboration, regulatory frameworks, and the speed of program cycles (Fig. 1).

We are entering a period of rapid change in the way that geoscience is embedded into the decision processes of mineral discovery and mining. There are as many barriers to adoption in processes and people, as implementation of smart technology. Future research needs to be more adept at delivering the results in the context of practical application, change management and systems. Regulatory frameworks inside and external to the business need to address the speed of decision making, the dynamic nature of exploration drilling and the potential to minimise environmental impact.

Agile exploration will be a paradigm that delivers greater value, reduced risk and better shareholder return. Technology is needed to deliver this framework, but people and systems will need to adapt to new and different processes. Core to all of this is better quality, quantitative, technology savvy and numerical geoscience. Are we as a community (academia, industry, METS and government) ready for this change?

Acknowledgements

This abstract has benefited from many conversations, discussions and training used in my job as a Product Manager.

References

Cleverley JS, Carey M, and Witherly, K, 2017. Decisions and Discovery – Upgrading to “Truth Machine 2.0”. SEG Newsletter, No. 109, p21-22

Noble R, Gonzalez-Alvarez I, Reid N, Krapf C, Pinchand T, Fox D, Ibrahimi T, Cole D, and Lau I, 2019. Coompana geochemistry – results from rapid surface characterization and a deep vertical profile. MESA Journal, 89(1): 4-14.

A Comparison of random forests and cluster analysis to identify ore deposits type using LA-ICPMS analysis of pyrite

Daniel D. Gregory
Department of Earth Sciences, Earth Sciences Centre, Toronto, Canada

Chao Liu, Shaunna M. Morrison, Robert M. Hazen
Carnegie Institution for Science, Washington DC, USA

Mathew J. Cracknell, Ross R. Large, Peter McGoldrick, Stephen Kuhn, Michael J. Baker, Nathan Fox, Ivan Belousov, Jeffery A. Steadman
ARC Research Hub for Transforming the Mining Value Chain, CODES, University of Tasmania, Australia.

Adrian J. Fabris
Geological Survey of South Australia, Department of the Premier and Cabinet, Adelaide, Australia

Valery V. Maslennikov
Institute of Mineralogy, Urals Branch, Russian Academy of Sciences, Russia.

Timothy W. Lyons, Maria C. Figueroa
Department of Earth Sciences, University of California, Riverside, California, USA.

Abstract. As exploration for new resources increasingly relies upon deeper and deeper drilling to investigate through overburden, exploration projects will encounter significantly higher drilling costs to sample target areas and to open new areas to exploration. Therefore, as much information as possible must be extracted from every drill hole. One tool that can be used is the in situ trace element analysis of individual mineral phases using LA-ICPMS. In this study, we investigate the use of pyrite trace element chemistry to fingerprint different ore deposit types so that appropriate geologic models can be employed at an early stage of exploration in new greenfields areas. While this data is effective at identifying ore deposit type, variability within the raw data leads to inherent complications for manual analysis. One way to deconvolute this data is to employ machine learning algorithms to aid in the classification. Here we develop a classifier using supervised classification (Random Forests) and further test non-supervised classification (cluster analysis) algorithms. The results of using Random Forests and cluster analysis to identify ore deposit type are then compared.

1 Introduction

Exploring though thick unmineralized cover is costly, and leads to difficulties in determining the correct geologic model to apply from a single intersection of mineralization. Application of new analytical tools are needed to help determine the type of mineralization at early exploration stages to identify potentially fertile ground. This will be useful for projects such as the co-funded drill holes currently being drilled in a regional context in Australia. The development of such a tool is the goal of this study.

The trace element content of pyrite is dictated by both the trace element content of the fluid from which the pyrite formed and the way in which pyrite was precipitated. Different ore deposit styles have different fluid compositions and precipitation mechanisms; thus it should be possible to use pyrite chemistry to identify ore deposit type. However, the trace element content can be complicated (Fig. 1) when viewing binary chemical plots and trying to classify deposit type manually. In this study we implement supervised machine learning (Random Forests) to identify ore deposit type using pyrite chemistry. This has been recently accepted for publication in Economic Geology (Gregory et al., *in press*). Here we further examine the results of un-supervised cluster analysis of the dataset.

2 The data repository

2.1 Laser ablation ICPMS

This project relies on LA-ICPMS analysis of the trace element content of pyrite. All analyses were carried out at the University of Tasmania, except some of the SEDEX analyses collected by Gadd et al. (2014) at Queen's University. Generally, each LA-ICPMS analysis used a 10-100 µm beam size and consisted of a 30s background measurement prior to a 40-60s period where the laser was turned on and material was ablated in a He atmosphere. The standard STDGL2b2 (Danyushevsky et al. 2011) was analyzed at the start

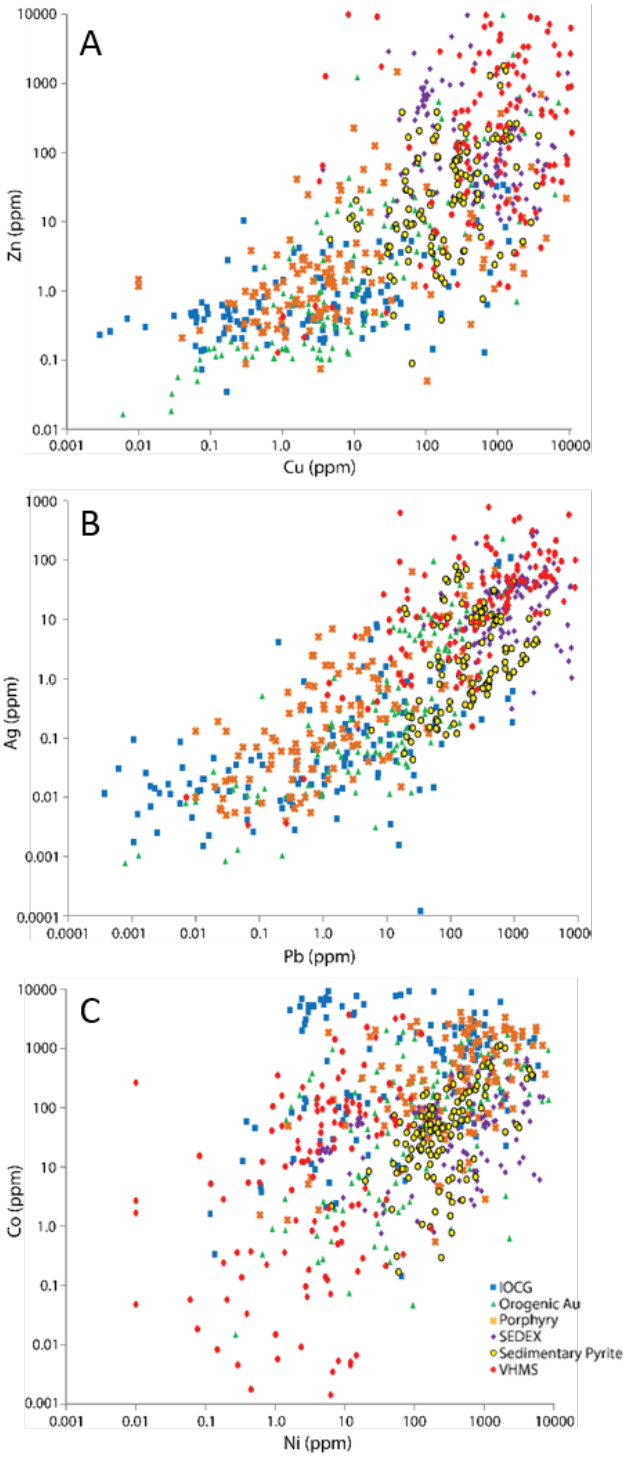

Figure 1: Trace element plots for training dataset for A) Zn vs Cu, B) Ag vs Pb, and C) Co vs Ni. Note that while the different deposits tend to fall within general areas there is high overlap between the different deposits.

and end of each analytical run (except for the analyses of Gadd et al. 2016, who used different standards) and approximately every 25 analyses in between.

A total of 3579 pyrite analyses were collated from IOCG, orogenic gold, porphyry Cu-Au, SEDEX and VHMS deposits and from barren sedimentary pyrite. These data were compiled from a variety of sources, including published papers, PhD theses, industry reports, and new data completed during this study see Gregory et al. (*in press*) for detailed reference list.

3 The Classifiers

3.1 Random Forests

To develop the classifier three main steps were utilized. First data were compiled and preprocessed; second the classifier was trained; and third the classifiers predictions were evaluated. The primary method employed here to develop the classifier of ore deposits based on the trace element abundance of pyrite utilizes supervised classification, namely Random Forests. Random Forests works by utilizing a large number of random decision trees (500 were used here) at each node of the decision tree the data set is split based on its trace element content after which it goes to another branch where it is further split until it reaches a level where a determination of the type of deposit the pyrite came from is made, based on a training data set of known deposit type. This work flow is carried out in different permutations by each of the trees. After which each tree votes for the deposit it thinks a given unknown is from and the deposit with the most votes is the one that is ultimately chosen.

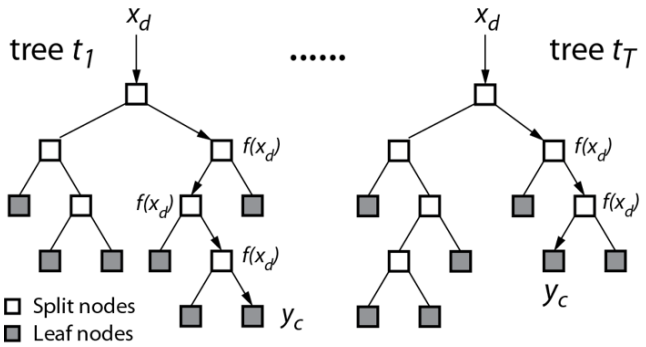

Figure 2: Diagram of the random forest. Each node of the decision tree the data set was split up to 5 times based on trace element content. We used a total of 500 decision trees.

Pyrite trace element data from 43 different deposits and barren sedimentary formations (2 IOCG, 15 orogenic gold, 2 porphyry Cu-Au, 5 SEDEX, 7 VHMS and 12 sedimentary formations were used to train the classifier. Where possible equal numbers of analyses from each deposit were used to avoid biasing the classifier towards a single deposit.

The classifier was tested in two different ways. First, additional data from the same deposits that were used to train the classifier (but not the same analyses) were used to do initial testing and refinement of the classifier. After successful initial testing a second set of data, from deposits that were not used in the training of the classifier, were used as a blind test. There was not enough data in this subset to conduct a blind test of each deposit type but we did have 681 analyses from 27 deposits and barren sedimentary formation (4 orogenic gold, 3

SEDEX, 17 sedimentary pyrite, and 3 VHMS). These analyses were put through the Random Forest classifier and the results were checked to see how well the classifier worked for a complete unknown. After classification the results were refined by removing all the classifications where the designated class received fewer than 40% of the votes from the Random Forest.

3.2 Cluster analysis

In this study we also tested clustering analysis of the pyrites based on their trace element concentrations. Various clustering techniques were tested, including K-Means, Gaussian Mixture Models, Affinity Propagation, Agglomerative Clustering, DBSCAN and so on. These are all unsupervised machine-learning models, i.e., the performance and rationality of the models can only be evaluated by domain knowledge, which, in this case, is our current understanding of pyrite paragenesis. Based on this approach, we discovered that the Gaussian Mixture model best described the clustering of pyrites in the database.

The Gaussian mixture model is a probabilistic model that assumes all the data points are generated from a mixture of a designated number (K clusters) of Gaussian distributions. The model is built and updated in a stepwise estimation-maximization process. Initially, values randomly selected within the data range are assigned for parameters of the K Gaussian distributions in the model. Based on these parameters, the probabilities of each data point following all K Gaussian distributions are calculated, and the highest probability determines which cluster (distribution) the data points belong to. Parameters of the distribution describing each cluster are then updated based on all the data points in that cluster, and then probability of all data points are calculated again based on the updated distribution parameters, and so on, until the result converges.

4 Results of the Classifiers

4.1 Results of the Test data

The results of the initial testing of the classifier were promising with all fields being classified correctly 86 to 99% of the time. Of particular interest is that the sedimentary pyrite, the stand in for "background" barren pyrite, was correctly identified 99% of the time, suggesting the classifier is effective at identifying unmineralized settings. For Tables 1 to 3, the following abbreviations are used: IG – IOCG, OG – orogenic gold, P – porphyry, SX – SEDEX, S – barren sedimentary pyrite, VS – VHMS.

Table 1. Confusion matrix for Random Forest classification of Test data

		Predicted						
		IG	OG	P	SX	S	VS	% correct
Actual	IG	**35**		1		1		95
	OG	7	**145**	16			1	86
	P	5	18	**216**		4	3	88
	SX			3	**623**	25	2	95
	S			1	4	**598**	4	99
	VS	1	7	1	4	3	**279**	95

4.2 Results of the Blind Test data

Similarly, to the test data, the results of the blind test classifications were also promising. The classifier correctly identified which deposit a pyrite analysis came from 85 to 97% of the time. Because several analyses are taken for each deposit, this represents a significant ability of the classifier to identify unknown mineralization styles. Furthermore, again the barren sedimentary pyrite was most effectively identified (97%) by the classifier suggesting it will be useful to separate background pyrite crystals from those related to mineralization.

Table 2. Confusion matrix for Random Forest classification of Blind Test data

		Predicted						
		IG	OG	P	SX	S	VS	% correct
Actual	IG	2						NA
	OG		**94**	8			6	86
	P							NA
	SX				**62**	2		97
	S	1		5	6	**378**	1	97
	VS	1	3	1	1		**33**	85

4.3 Effect of untrained data on the classifier

One problem with using a supervised classifier, such as Random Forests, is that it will always give an answer, thus if a sample is from an origin that is not one of the groups in the training set, a spurious result will be generated (i.e. the classifier will pick the closest category in the training dataset). To check whether pyrite types not represented in the training dataset can be identified as such by the classifier, we put a dataset from the St Ives gold district that has 7 different types of pyrite, 2 of sedimentary origin and 1 associated with the gold mineralization but 4 more not related to mineralization (Gregory et al. 2016). We established the criteria that for a conclusive designation at least two thirds of the analyses must be also be conclusive (i.e. received >40% of votes from the Random Forest). The sedimentary pyrite and orogenic Au were conclusively, correctly identified and 3 of the 4 non-mineralized pyrite

parageneses were inconclusive; which they should be as their correct designation was not represented in the training data set (Table 3). However, one pyrite type was incorrectly conclusively designated as orogenic Au. This shows that more data, from different pyrite types, needs to be accumulated to refine the classifier.

Table 3. Random Forest classification of pyrite from St Ives Gold district (Gregory et al. 2016)

Pyrite type	% inconclusive	% most common classification	Most common classification
Sedimentary	16	97.5	Sedimentary
Py3	14	62.5	Orogenic Au
Py4	38	80.0	Orogenic Au
Py5	76	100.0	Porphyry
Orogenic Au	9	84.9	Orogenic Au
Py7	20	62.5	Porphyry

4.4 Results of the Cluster Analysis

Using a Gaussian Mixture Model 7 different classes were identified using the cluster analysis. In general, the cluster analysis separated most of the pyrite types, similar to the Random Forest. Yet there was more overlap evident between the different fields, especially between a subgroup of porphyry and orogenic Au (Fig. 3). The reason for this is not readily apparent and will be the focus of further investigation.

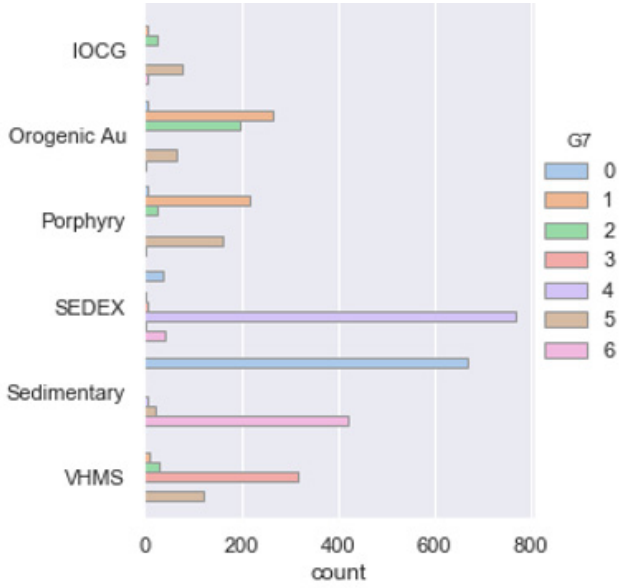

Figure 3: The different clusters identified in the cluster analysis and which deposits most commonly were associated with different clusters. Note SEDEX, Sedimentary, and VHMS are largely within their own groups whereas the higher temperature pyrite are largely separated have much more overlap.

5 Discussion

The high degree of correct classification and the ability to determine that pyrite types not in the training set are inconclusive in most cases suggests the use of Random Forest classification is a useful tool when combined with other methods, to identify mineralization styles in unknown samples. However, it also highlights the need to acquire more data from other deposits types (i.e. epithermal gold, Carlin etc.) and to obtain data from unmineralized pyrite to strengthen the classifier before it can be robustly applied in an exploration context.

The results were supported by the cluster analysis. However, the cluster analysis had more difficulty in separating the higher temperature varieties of pyrite. The results were still encouraging as they supported the random forest results and are likely better at identifying pyrite types that are not part of the training set. Thus, going forward we will investigate using the two techniques in conjunction with one another.

Acknowledgements

This project arose out of funding from the Geological Surveys of Western Australia and South Australia for initial data collection and testing of the classifier. Additionally, data was also obtained from the AMIRA P1060 project. The NSF FESD Program and the NASA Astrobiology Institute under Cooperative Agreement No. NNA15BB03A issued through the Science Mission Directorate provided funding for the development of the classifier and mining of pyrite data from literature sources.

References

Danyushevsky, L., Robinson, P., Gilbert, S., Norman, M., Large, R., McGoldrick, P., and Shelley, M. (2011) Routine quantitative multi-element analysis of sulphide minerals by laser ablation ICP-MS: Standard development and consideration of matrix effects. Geochemistry: Exploration, Environment, Analysis 11:51-60.

Gadd, M. G., Layton-Matthews, D., Peter, J. M., and Paradis, S. J. (2016) The world-class Howard's Pass SEDEX Zn-Pb district, Selwyn Basin, Yukon. Part I: trace element compositions of pyrite record input of hydrothermal, diagenetic, and metamorphic fluids to mineralization. Mineralium Deposita 51:319-342.

Gregory, D. D., Large, R. R., Bath, A. B., Steadman, J. A., Wu, S., Danyushevsky, L., Bull, S. W., Holden, P., and Ireland, T. R. (2016) Trace Element Content of Pyrite from the Kapai Slate, St. Ives Gold District, Western Australia. Econ Geol 111:1297-1320.

Gregory, D. D., Cracknell, M.J., Large, R. R., McGoldrick, P., Kuhn, S., Maslennikov, V.V., Baker, M.J., Fox, N., Belousov, I., Figueroa, M.C., Steadman, J.A., Fabris, A.J., and Lyons, T.W. (*in press*) Distinguishing ore deposit type and barren sedimentary pyrite using LA-ICPMS trace element data and statistical analysis of large datasets. Econ Geol.

3D ore prediction by MLAs based on computational modeling in maturely explored area: a case study in Anqing orefield, China

Liu Liangming, Qin Yaozhu
Computational Geosciences Research Center, Central South University

Abstract. In a maturely explored area, it is difficult to select targets with high potential to be drilled further, because there are so many factors disturbing the exploration and ore prediction. The Anqing orefield is such an area. Although the early geophysical works led to the initial discovery of ore deposits in this orefield, the recent intensive geophysical exploration failed to find new orebodies. For evaluating the exploration strategy based on geophysical data and facilitating discovery of hidden orebodies, we apply the random forests (RF), one robust method of the machine learning algorithms (MLAs), to process the data from both the geophysical surveying and computational modeling on geometry and geodynamics of the ore-controlling intrusion. The study not only explains why no orebodies have been discovered by drilling the geophysical anomalies, but also predicts locations with high potential in 3D. The existing orebodies absolutely occur in the locations with high prospectivity. The high prospectivity locations that have not been drilled must be the targets to be drilled further. Such prospective targets are mainly in the western segment of the intrusion's contact zone.

1 Introduction

Prediction of hidden orebodies is generally not so easy and does not necessarily leads to successful discoveries, especially in the maturely explored setting. The critical impediments to the successful ore prediction are from the exploration data and the prospectivity modeling techniques, because the data are absolutely influenced by a lot of factors and their association with the orebodies is very complicated, and usually nonlinear (Qin and Liu 2018). With the rapid growth of computing power, the MLAs have been developed as a group of robust methods for conducting sound prospectivity model by analyzing the complex relationship between multitude evidential features and mineralization (Rodriguez-Galiano et al. 2015; Xiong et al. 2018). It has been demonstrated that MLAs are more accurate than statistical techniques commonly used in ore prediction, especially when the multi-sourced data with different statistical distributions are used. MLAs have the potential to identify and model the complex non-linear relationships between the mineral occurrences and the evidential features (Bwown et al. 2000).

The Anqing orefield, with the largest Fe-Cu skarn deposit in the Yangtze River metallogenic belt (YRMB), is a maturely explored area. The ore deposits in this field were initially discovered by drilling in the magnetic anomalies in 1959 (Liu et al. 2011, 2012). However, its recent exploration strategy for finding hidden orebodies at depth was not successful. Twelve deep drillholes were finished at the targets delineated by the Controlled Source Audio-frequency Magnetotelluric (CSAMT) data, but no orebody was discovered. For finding a way out of such awkward situation and facilitating ore discovery, we simulate the geometric shape and cooling dynamic process of the ore-controlling intrusion, and use the RF to predict the hidden orebodies.

2 Geological setting and current situation of exploration

2.1 Geological setting

The Anqing orefield is located in the middle of YRMB. The orebodies in this field are mainly Cu and Cu-Fe skarns, minor Fe skarns, occurring in the contact zone between the Yueshan intrusion and marble and dolomite marble of the low to mid Tertiary age (Fig.1). Hundreds of orebodies have more than 48.8 Mt @ 1.3% Cu ores and 100 Mt @ 48% Fe ores.

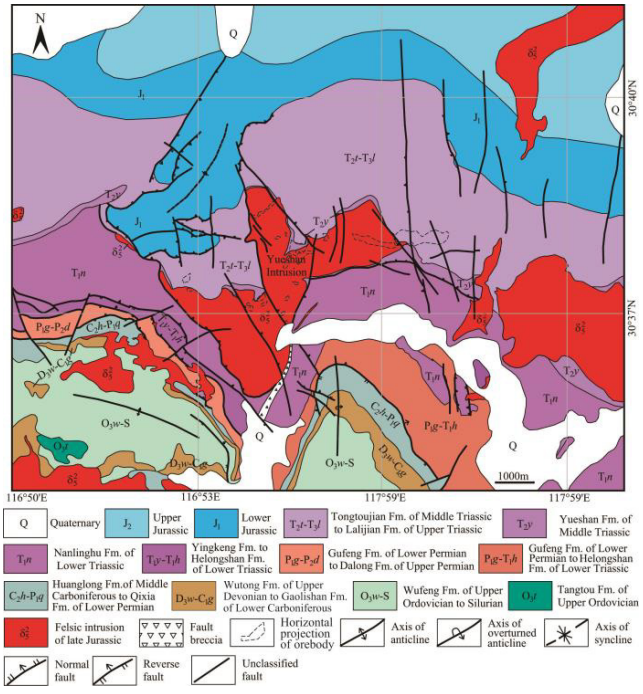

Figure 1. Geological map of Anqing orefield (modifying from Liu et al. 2012).

The Yueshan intrusion is the key ore-controlling factor in this orefield (Figs.1 and 2). It is irregular shaped and composed mostly of diorite with minor quartz diorite, with U–Pb zircon isotopic age of 138.7 Ma (or Mid Early Cretaceous). The geological and geochemical features of the intrusion and ore deposits indicate that mineralization took place during the cooling process of the intrusion (Liu et al. 2011, 2012). The orebodies are distributed very unevenly along the contact zone (Fig.2a). The ore distribution is obviously related to geometric and topographic features of the intrusion (comparing Fig.2a with Fig.2b). The E-W trending contact zones with rough irregular surface are favorable for localization of orebodies.

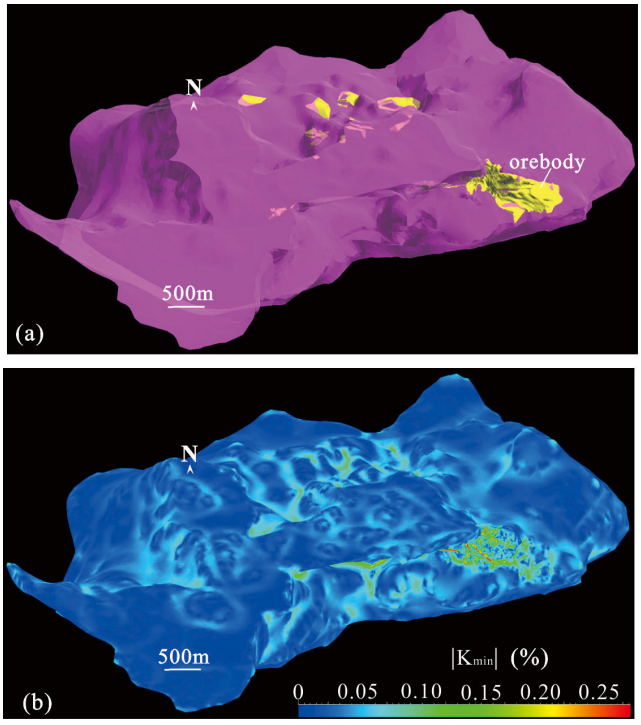

Figure 2. (a) Yueshan intrusion and orebodies along its contact zone; (b) variation of Gaussian curvature of the Yueshan intrusion's contact surface

2.2 Current situation of exploration

The Anqing orefield has been maturely explored and mined. Since the first drilhole in 1959, more than 1200 drillholes with a total length of more than 370000 m and more than 110000 m underground tunnels have been finished there. These works have provided abundant information of the underground geology and led to discovery of lots of orebodies as well. For increasing ore reserves through deep exploration, a recent program of CSAMT survey of 26.6 km^2 was carried out on a grid spacing of 200m×40m within the orefield. Targeting at the low resistivities detected by CSAMT, the 12 drill holes with accumulative depth of 16725.39m have been finished. Unfortunately, no orebody has been discovered by these works, demonstrating that the CSAMT is not effective enough to discover hidden orebodies at depth. Nowadays it is necessary to explain why the CSAMT data are not capable of giving credible prediction and to find a capable method for facilitating predictive discovery of orebodies at depth.

3 Computational modeling

To understand the spatial structures of mineralization system, we construct the 3D surface-based models of Yueshan intrusion, orebodies and carbonate wall rocks by using geological data from all exploration works. In the 3D models, we use Delaunay algorithm to construct a triangulated irregular network (TIN) to model the inter-surfaces of geological bodies, and optimize the modeling surfaces by using the DSI (discrete smooth interpolation) algorithm. The models show that the locations of orebodies are closely related to the geometric and topographic features of the intrusion (Fig.2).

As the mineralization was simultaneous with the retrograde alteration, the orebodies must have been formed during cooling process of the Yueshan intrusion. Using the finite difference algorithm in the platform of FLAC3D, we model the syn-stretching cooling process of the Yueshan intrusion (Liu et al. 2012). The modeling results show that the dilatant deformation is favorable for localization of orebodies (Fig.3)

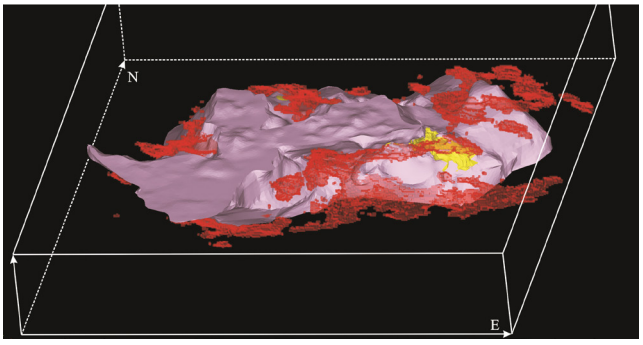

Figure 3. Showing spatial association of orebodies (yellow) with intrusion (pink) and dilation zones with volume strain >0.8% (red)

4 Random forest algorithm

The MLAs are increasingly applied to achieve interpretation, classification and prediction in geological exploration, as they can simultaneously use multiple variables to reduce interpretation bias and outperform the traditional graphical or statistical methods (Friedman et al. 2001; O'Brien et al. 2015; Kirkwood et al. 2016; Caté et al. 2018). The most widely used MLAs include decision trees (DT) (Breidman et al. 1984), artificial neural networks (ANN) (Brown et al. 2000), support vector machine (SVM) (Abedi et al. 2012) and random forest (RF) (Breiman 2001).

The RF, an ensemble DT algorithm, combines the performance of numerous DT algorithms to classify or predict the value of a variable (Breiman 2001; Carranza and Laborte 2015). Each decision tree is built from a sample of the training set (bootstrapping) and a random portion of the discriminative variables are used at each

split. For avoiding the correlation of the different trees, RF increases the diversity of the trees by making them grow from different training data subsets created through a procedure called "bagging". Bagging generates training data for each tree by sampling with replacement a number of samples equal to the number of samples in the source dataset, i.e., with no deletion of the data selected from the input sample for generating the next subset. Hence, some data may be used more than once in the training, while others might never be used. Thus, greater stability is achieved, as it makes it more robust when facing slight variations in input data and, at the same time, it increases prediction accuracy (Breiman 2001). RF implements the Gini Iindex to determine a “best split” threshold of input values for given classes. The Gini Index returns a measure of class heterogeneity within child nodes as compared to the parent node (Breiman et al.1984; Waskeetal 2009; Cracknell and Reading 2014).

5 Geological and geophysical data for RS

The data inputted for RS calculation are of 4 different features, or 4 vairiables: (1) volume strain produced by computational dynamic modeling; (2) curvature of the intrusion’s contact surface; (3) electric resistivity detected by CSAMT surveying; (4) wall rocks (carbonate or not).

The CSAMT surveying had only been carried out only in the eastern part of the orefield. The orebodies are not closely associated with low resistivities detected by CSAMT (Fig. 4).

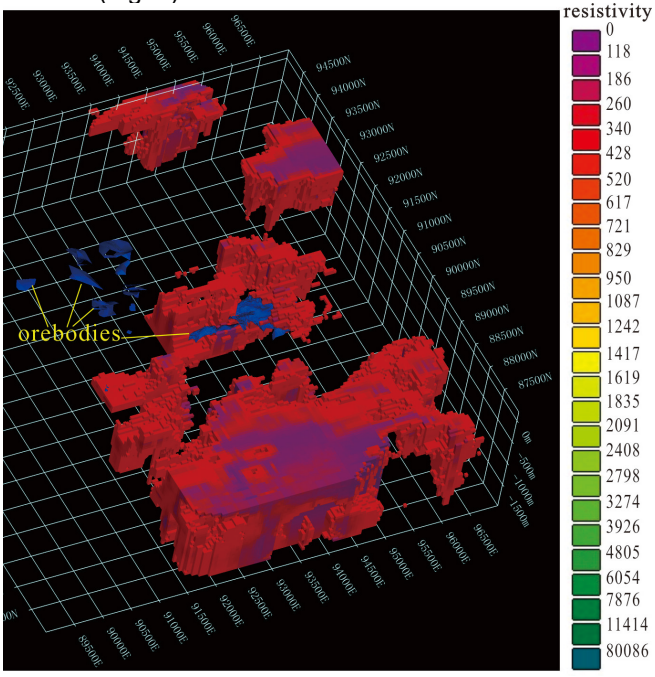

Figure 4. Low resistivity (<500 Ω.m) and orebodies

6 3D prospectivity model by RF

In the eastern part of the orefield, the data of all 4 variables including resistivity are available. The domain is divided into 719459 cubes, among which 1986 cubes are occupied by ores, 11543 cubes have been drilled but no orebodies discovered, and 715687 cubes have not been drilled. 70% of mineralized cubes and 70% of un-mineralized cubes are selected randomly as training sets. The RF calculation produce the 3D prospectivity model as Fig.5. The high prospective zones with high probability of having ores are distinctly different from the low resistivity spaces (Figs. 4 and 5). The orebodies already discovered are all located in the high probable zones (Fig. 5).

Because the CSAMT surveying has not covered the whole orefield, the electric resistivity data are not available to process RF calculation in the whole orefield. The whole orefield is divided into 2061067 cubes, among which 3186 cubes are occupied by ores, 14071 cubes have been drilled but no orebodies discovered, and 715687 cubes have not been drilled. 70% of mineralized cubes and 70% of un-mineralized cubes are selected randomly as training sets. The RF prediction model is set up by considering 3 variables, volume strain, geometric features of intrusion’s contact surface and wall rocks. The 3D prospectivity model of RF (Fig. 6) shows that the exiting orebodies are all localized in the high potential zones. The high potential zones that have not been drilled must be prospective targets that are worthy to be drilled further for discovering hidden orebodies. Such prospective targets are mainly in the western segment of the intrusion’s contact zone where the contact surface is concaved inward (Fig. 6).

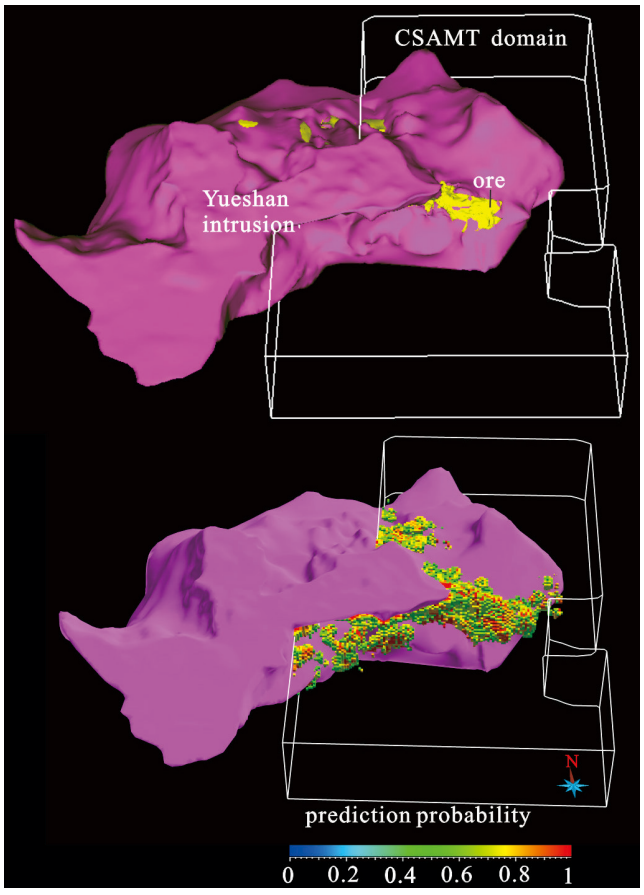

Figure 5. Prediction probability in the domain with CSAMT surveying

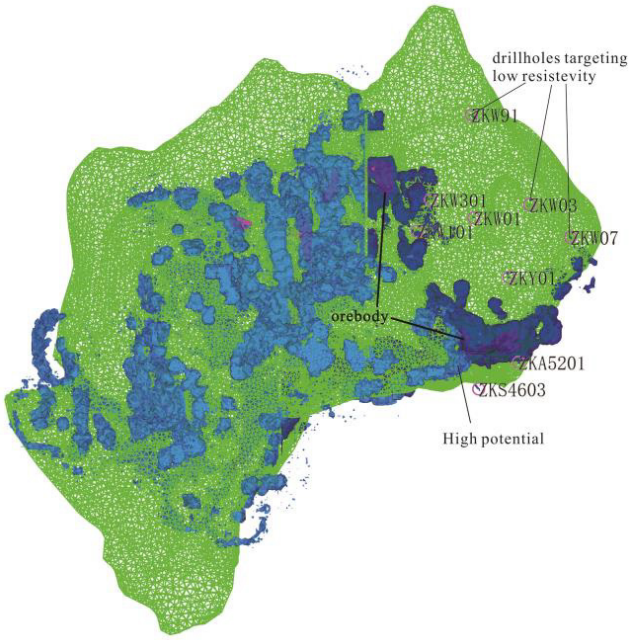

Figure 6. High potential zones predicted by RS model in the whole orefield

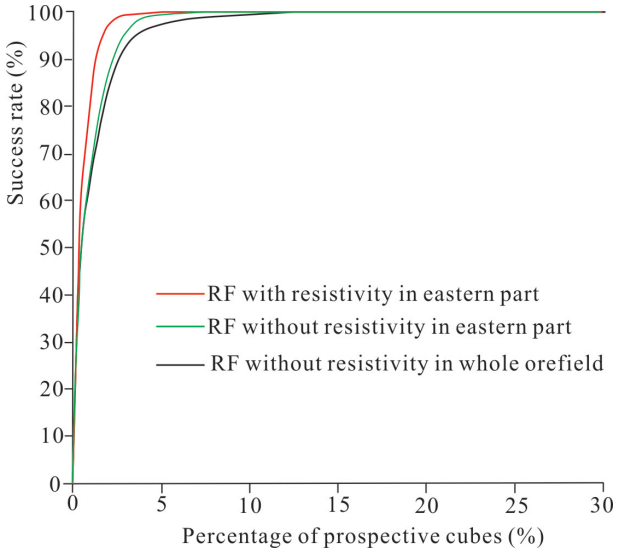

Figure 7. Mineral prospectivity success of the 3D mineral potential models respectively in eastern part and whole orefield

Although the RF model with resistivity data has a better success rate than RF models without resistivity data, all models have successful behavior (Fig. 7). For percentage threshold values of prospective cubes over 3%, the success rate of RF is over 90%. No matter whether or not using the variable of resistivity, the RF models give the almost same prediction (Figs.5 and 6). It suggests that the CSAMT surveying has little contribution to the ore prediction. The possible reason for such situation is that the CSAMT data are strongly influenced by the noisy background. All the drillholes targeting at the low resistivity are not in the high potential zones predicted by RF models (Figs. 5 and 6). The RF prediction results demonstrate that the MLAs are useful for constructing sound exploration strategy in the maturely explored setting.

Acknowledgements

Research funding was provided by the NSFC through grants awarded to Liu (grants No. 41372338 and No. 41772351). We acknowledge the Tongling Nonferrous Metal Group Ltd. Company for the financial and logistic support during the field work.

References

Abedi M, Norouzi GH, Bahroudi A (2012) Support vector machine for multi-classification of mineral prospectivity areas. Comput Geosci 46: 272–283.

Breiman L (2001) Random forests. Mach Learn 45: 5–32.

Breiman L, FriedmanJ, Stone CJ, Olshen RA (1984) Classification and Regression Trees.1st ed. Chapman and Hall/CRC, Belmont, CA.

Brown WM, Gedeon TD, Groves DI, Barnes RG (2000) Artificial neural networks: a new method for mineral prospectivity mapping. Aust J Earth Sci 47: 757-770.

Carranza EJM, Laborte AG (2015) Random forest predictive modeling of mineral prospectivity with small number of prospects and data with missing values in Abra (Philippines). Comput Geosci 74: 60-70.

Caté A, Schetselaar E, Mercier-Langevin P, Ross P-S (2018) Classification of lithostratigraphic and alteration units from drillhole lithogeochemical data using machine learning: A case study from the Lalor volcanogenic massive sulphide deposit, Snow Lake, Manitoba, Canada. J Geochem Explor 188: 216–228.

Cracknell MJ, Reading AM (2014) Geological mapping using remote sensing data: Acomparison of five machine learning algorithms, their response to variations in the spatial distribution of training data and the use of explicit spatial information. Comput Geosci 63: 22–33.

Friedman J, Hastie T, Tibshirani R (2001.) The Elements of Statistical Learning. Springer, Berlin (533 pp).

Kirkwood C, Cave M, Beamish D, Grebby S, Ferreira A (2016) A machine learning approach to geochemical mapping. J Geochem Explor 167: 49–61.

Liu LM, Wan CL, Zhao CB, Zhao YL (2011) Geodynamic constraints on orebody localization in the Anqing orefield, China: Computational modeling and facilitating predictive exploration of deep deposits. Ore Geo Rev 43: 249-263.

Liu LM, Zhao YL, Sun T (2012) 3D computational shape- and cooling process-modeling of magmatic intrusion and its implication for genesis and exploration of intrusion-related ore deposits: an example from the Yueshan intrusion in Anqing, China. Tectonophysics 526-529: 110-123.

O'Brien JJ, Spry PG, Nettleton D, Xu R, Teale GS (2015) Using Random Forests to distinguish gahnite compositions as an exploration guide to Broken Hill-type Pb–Zn–Ag deposits in the Broken Hill domain, Australia. J Geochem Explor 149: 74–86.

Qin YZ, Liu LM (2018) Quantitative 3D Association of Geological Factors and Geophysical Fields with Mineralization and Its Significance for Ore Prediction: An Example fromAnqing Orefield, China. Mineral, 8 (300):1-23.

Rodriguez-Galiano V Sanchez-Castillo M, Chica-Olmo M, Chica-Rivas M (2015) Machine learning predictive models for mineral prospectivity: An evaluation of neural networks, random forest, regression trees and support vector machines. Ore Geol Rev 71: 804-811

Xiong Y, Zuo R, Carranza EJM (2018) Mapping mineral prospectivity through big data analytics and a deep learning algorithm. Ore Geol Rev 102: 811-817

Building 3D geomodels using XRF-XRT-generated drill core data: The Lovisa-Håkansboda base metal- and Strássa-Blanka iron deposits in Bergslagen, Sweden

Stefan Luth[1,2], Fredrik Sahlström[2], Nils Jansson[3], Johan Jönberger[1], Stefan Sädbom[4,5], Eric Landström[5], Mikael Bergqvist[5], Nikolaos Arvanitidis[1], Ronald Arvidsson[1]
[1]Department of Mineral Resources, Geological Survey of Sweden, Sweden
[2]Department of Earth Sciences, Uppsala University, Sweden
[3]Division of Geosciences and Environmental Engineering, Luleå University of Technology, Sweden
[4]Lovisagruvan AB, Sweden
[5]Orexplore AB, Sweden

Abstract. 3D geological models based on data from geological field observations, magnetic airborne surveys and combined XRF-XRT scanning of drill core are presented for the Lovisa-Håkansboda and the Strássa-Blanka mineral systems (1.9 - 1.8 Ga). At first, the 3D architecture of several deposits was derived primarily from surface data and mine-level maps. Secondly, geochemical and structural constrains from drill core scanning (XRF-XRT) were used to refine the models locally to a detailed, in-mine scale. The constructed models were then placed in a regional context providing valuable insight on the area's local and regional deformation pattern. All modelled deposits are plunging 50-60° towards the south-southeast reflecting D2 deformation (vertical shearing) during NW-SE-directed shortening and are locally overprinted by D3 (lateral shearing) during N-S-directed shortening.

1 Introduction

Various sulphide mineralizations of different types (Zn-Pb-Ag and Cu-Co) occur within short distances in the Lovisa-Håkansboda area (4 km^2). Despite the long mining history in the area and its high potential for several critical metals including silver, gold, cobalt, antimony and bismuth, knowledge about the mineral system and ore genetic models is limited (e.g. Carlon and Bleeker 1988, Jansson et al. 2018). Difficulties arise from a high complexity in terms of chemistry, mineralogy, textures and metal content all varying within short distances. Additionally, a strong tectonic overprint mostly blurred primary features causing remobilization and secondary textures (Sahlström et al. 2019 this volume).

To resolve the area's structural complexity, in order to better understand the mineral system, an integrated approach is necessary and includes combining of various datasets. As such, access to in-mine infrastructure and drill cores needs to be combined with data from geological and geophysical surveys on a near-mine scale. In addition, valuable, high resolution geochemical and structural datasets can now easily be obtained from combined XRF-XRT drill core scanning (X-mine project, EU/Horizon 2020).

In this study, we investigate the structural setting of the Lovisa-Håkansboda base metal and Strássas-Blanka iron—oxide mineral systems by integrating new data from geological field observations, magnetic surveys, and XRF-XRT drillcore scanning. 3D deposit models are then constructed for each deposit. The modelled subsurface are analysed and evaluated in the light of structural control and regional deformation.

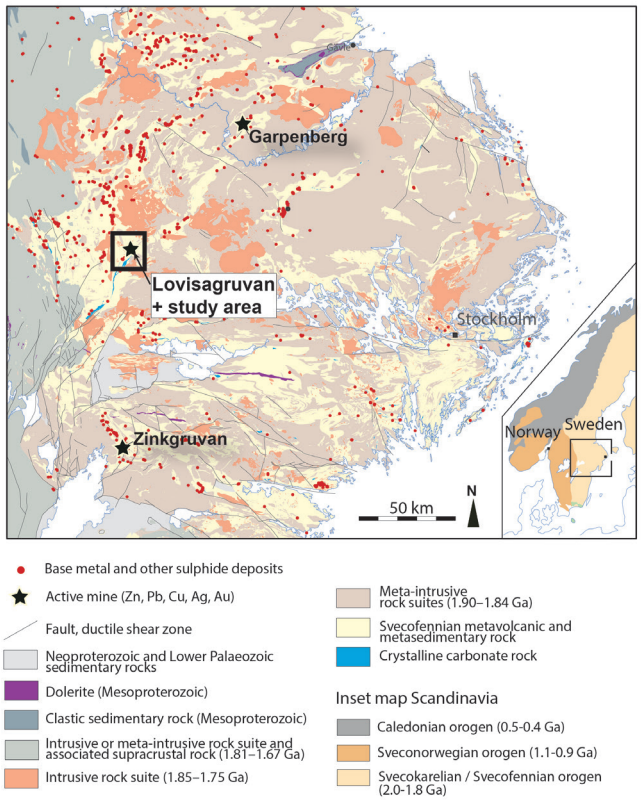

Figure 1. Geological map of the Bergslagen region including the outline of the study area. Inset shows the main tectonic domains in Norway and Sweden.).

2 Geological setting

The Bergslagen mining province is part of the Bergslagen lithotectonic unit of the Fennoscandian Shield (Stephens and Andersson 2015) (Fig. 1). The unit largely consists of syn-orogenic plutonic rocks intruded in a succession dominated by felsic metavolcanics rocks, which were

deposited in a continental back-arc basin during the Svecokarelian orogeny (1.9 – 1.8 Ga) (Stephens and Andersson 2015). The metavolcanic succession is interbedded by volcanoclastic mass flow deposits, limestone, BIFs and sulphide mineralization. Deformation was polyphase and metamorphism was low-pressure up to amphibolite facies during metamorphic peak conditions. Large-scale folding and shearing resulted in the formation of inliers of the supracrustal rocks, which became bounded by plutonic rocks and shear zones. A relatively large inlier in western Bergslagen is the 45 km long, NE-trending Guldsmedshyttan syncline, hosting many iron-oxide and base metal sulphide deposits along strike. The deposits for this study (Lovisa-Håkansboda, Stråssa-Blanka) are situated in the northern tip of the syncline (e.g. Lundström1983, Jansson et al. 2018).

2.1 The Lovisa Zn-Pb-(Ag) deposit

The Lovisa sulphide deposit on the western fold limb is actively mined with a reserve of 675 000 tons ore with zinc (9,5%), lead (3,9%) and some silver (Lovisagruvan AB annual report 2018). The reserve is proven by 90 drill holes 1100 m along strike and down to 425 m and is open at depth and to the south.

The Lovisa deposit is stratiform and consists of two steeply dipping horizons (Jansson et al. 2018). A laminated, sphalerite-dominated “Sphalerite Ore” (>15% Zn) and a horizon of galena-dominated “Main ore” (>40% Zn+Pb). The ore layers are separated by a 1 to 3 meters wide zone of barren rock (< 1% Zn+Pb). The total thickness of the ore layers varies between less than 1 m to up to 3 meters. The host rock as well as the interbedded layers between the ore layers are rhyolitic ash siltstones and chloritic schists. The formation of stratiform ore layers is interpreted as syn-genetically in a vent-distal, seafloor exhalative setting (Jansson et al. 2018). Subsequently the ore layers and the surrounding rocks became metamorphosed to upper amphibolite facies and ductile and brittle deformed resulting in post-genetic ore textures (e.g. metablastic growth, shearing and folding, mineral intergrowth) and remobilization (Sahlström et al. 2019 this volume).

2.2 The Håkansboda (Cu-Co-As-Bi-Au) deposit

The Håkansboda deposit is hosted by massive limestones with interbeds of calc-silicate rocks and rhyolitic ash siltstone and is interpreted to occur on the eastern fold limb and stratigraphically below the stratiform Lovisa deposit (Lundström, 1983; Carlon & Bleeker 1988). Mineralization is known for 850 m along strike and to a depth of 600 m but is open at depth and to the south. The indicated reserve is 629.000 tons of 1,4% Cu, 0,4 g/t Au and 14,3 g/t Ag (in-situ grades) (Kopparberg Mineral AB, 2012). The dominant ore minerals are chalcopyrite, cobaltite, glaucodot, arsenopyrite, pyrrhotite, pyrite, sphalerite and galena, and accessory bismuth minerals (e.g. Magnusson 1973). The ore occurs as massive lenses, schlieren or banded mineralisation, disseminated sulphides and as breccias. The ore textures indicate post-genetic deformation and remobilization (Carlon and Bleeker 1988). Carlon and Bleeker (1988) suggested that the Håkansboda deposit formed in a feeder zone for stratiform mineralization in the area (e.g. Lovisa deposit).

2.3 The Stråssa and Blanka (Fe-oxide) deposits

The Stråssa iron-oxide deposit consists mainly of quartz-magnetite and hematite ores with variable amounts of magnetite, hematite and skarn minerals (hornblende, diopside, epidote). The iron content varies between 25% and 45%. Sulphides (pyrite, chalcopyrite, and pyrrhotite) occur only locally within the iron ores at Stråssa, however, at Blanka, which is situated at the same stratigraphic horizon 1.7 km south of Stråssa, pyrite and chalcopyrite are more common and are observed mostly in the actinolite skarns (Koark, 1960). In addition, the iron ores from Blanka are less stratified than at Stråssa and intense deformation of the ore bodies resulted in discordant stocks, specularite-schists and large-scale mullions plunging 50° to the SE (Bleeker and Carlon 1988).

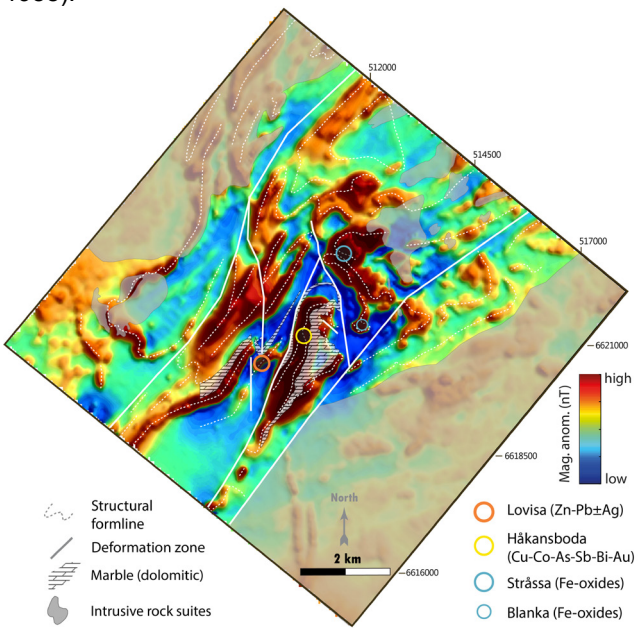

Figure 2. Deposits and main structural features projected onto the magnetic anomaly map based on airborne measurements (100 meters line spacing at 60 meters ground clearance).

3 Structural framework and 3D modelling

The Guldsmedshyttan syncline is the dominant regional structure, which is mostly NE-SW trending, steeply inclined, isoclinal and doubly plunging and locally overturned. In the Lovias-Håkansboda mining area the syncline is refolded along its northern tip (hook-shape) and is dismembered by predominantly NE to N trending shear zones and faults (Fig. 2). The syncline’s western fold limb comprises besides the relatively low magnetic metavolcanics rocks and carbonates, highly magnetic quartz banded iron formations and iron skarn horizons. These iron ore bearing layers stand out on the magnetic anomaly map and are often well traceable over long distances. Due to the high resolution of a recent airborne

magnetic survey (100 meters flight line spacing at 60 meters ground clearance) a complex folding pattern has been identified (Fig. 2). Additional field observations (e.g. structural measurements and strain indicators in outcrops and thin-sections) reveal that a large number of macroscopic folds are doubly plunging (locally even sheet folds) and fold a pre-exiting penetrative foliation (S1). The F2 folds are sheared and boudinaged vertically as well as elongated in an NE-SW direction parallel to the main trend of the Guldsmedshyttan syncline. The limbs are locally refolded (F3) by open to isoclinal S- or Z- folds along steeply to moderately south to southeast plunging fold axes. In terms of tectonic events, the overprint between F2 and F3 folding may be explained by a stage of reverse-shearing and vertical extrusion during D2 (NW-SE directed shortening) followed up by a wrenching phase (D3) of predominantly sub-horizontal shearing in both a sinistral and dextral sense during regional N-S directed shortening.

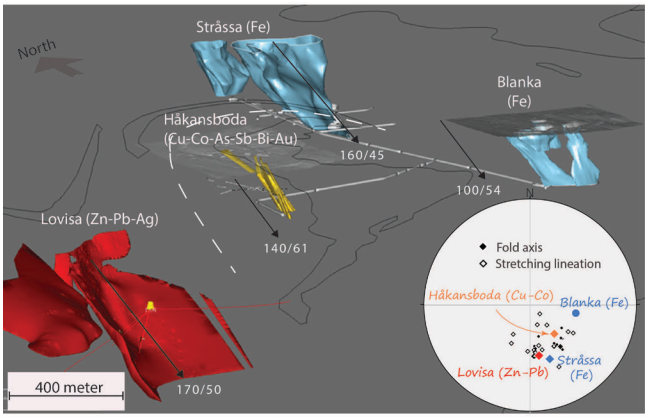

Figure 3. 3D outline of the modelled deposits at the north tip of the Guldsmedshyttan syncline. The dashed line refers to the map trace of the refolded syncline's axial plane. Stereogram in the lower right combines field measurements in the area with the average plunge of the deposits.

3.1 Construction and interpretation of the 3D ore deposit models

The 3D ore deposit models are primarily based on geological surface maps, structural measurements and mine maps from the active mining period (Fig. 3). Additionally, available drill core logs have been used mainly to test the models at depth.

The models reveal a distinctive outline for each deposit (Fig. 3). The Stråssa main iron orebody is strongly folded and tightens at depth plunging 45° to the southeast. At Blanka the ore bodies are located on separate fold limbs at shallow levels and merge downwards into a single ore body. Modelling of the Håkansboda ore shows several rod-shaped ore bodies that plunge moderately to steeply to the south-east. The Lovisa Zn-Pb-Ag ore body is tabular with a rather constant thickness of a few meters. The layer is gently folded around a fold axis plunging 50° to the south east (Fig. 3).

Despite the variation of the obtained geometries among the deposits, a typical feature of all deposits is their plunge of 45° to 60° towards the south-southeast. A similar structural trend is shown by the measured fold-axes and stretching lineations in the adjacent bedrock within the study area (Fig. 3). Steeply plunging, rod-shape geometries have been reported for several sulphide and iron-oxide ore deposits in the Bergslagen lithotectonic unit. (e.g. Kampmann et al. 2016). In line with Kampmann et al. (2016) we suggest that D_2 deformation of predominantly reverse shearing may have produced doubling plunging folds and cone to rod shaped ore bodies in a single deformation phase. Subsequently, strike-slip and horizontal shearing during D_3 caused locally refolding and thickening of low-viscosity zones, such as carbonate and ore bearing layers.

3.2 Using XRF-XRT drill core scanning to refine 3D deposit models

Additional constraints to the Lovisa (Zn-Pb-Ag) 3D deposit model were obtained from drill core scanning data combining XRF-XRT (Orexplore, in press). This innovative scanning technology was developed by the company Orexplore and detects both the rocks geochemical signature as well as its internal textures, structures and density through X-Ray Fluorescence (XRF) measurements and high-resolution 3D tomography from X-Ray Transmission (XRT). By modelling the material using minerals as building blocks and performing stoichiometry calculations, an assessment of the plausible mineral compositions can be made, as well as providing inferred values for non-measured elements. The development of a workflow integrating this advanced technology into exploration, including 3D geomodelling, is one of the two focus areas of the X-mine project, EU / Horizon 2020.

The real-time workflow (Fig. 4) starts in-mine where scanning can be performed at a speed in line with drilling and the preferred resolution. The obtained chemical, structural and textural data can then be analyzed, interpreted and exported into formats suitable for 3D geological modelling (Leapfrog, Move, Gocad etc.). After well correlation a detailed 3D model can be constructed serving as input for new targeting.

In the Lovisa mine, XRF-XRT scanning of drill core allowed for a more precise distinction between barren rock and the laminated zinc ore occurring within layers of typically less than a meter thick (Fig. 4).

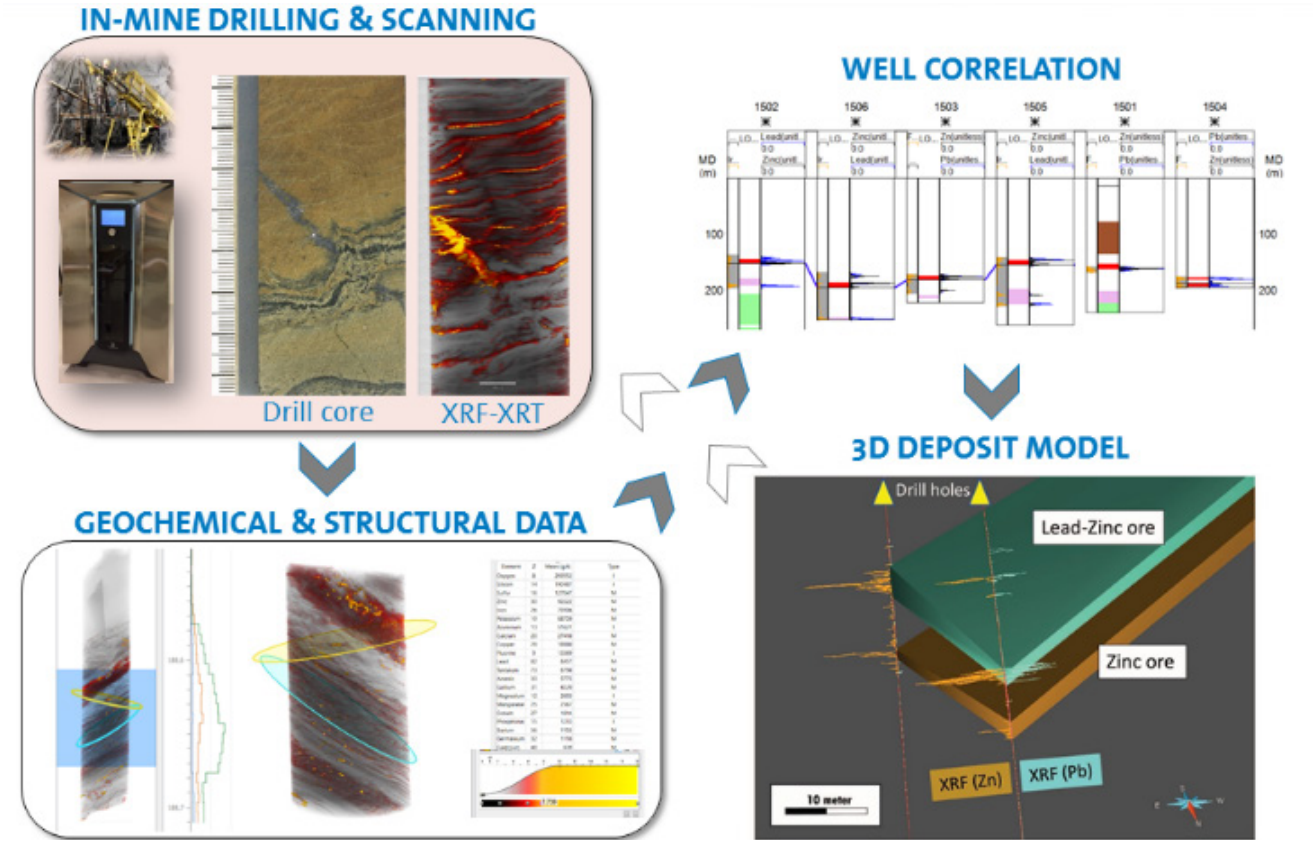

Figure 4. Real-time workflow integrating combined XRF-XRT scanning of drill core with 3D geomodelling of ore-deposits. In-mine scanning is performed directly after drilling (upper left), visualization and analysis of the obtained geochemical (XRF) and structural (tomography) data in the software Orexplore Insight (lower left), export of data and interpretations into 3D geomodelling applications allow then for accurate correlation (upper right) and the creation of 3D surfaces and property grids (lower right).

4 Conclusions

The structural setting of the Lovisa-Håkansboda and the Strássa-Blanka mineral system has been investigated utilizing geological field observations, magnetic airborne surveys and combined XRF-XRT scanning of drill core. The 3D structure of the ore deposits was extracted from mine-level maps and was then refined using high-resolution geochemical- and structural constraints derived from drill core scanning. In a regional context, the modelling results reveal a strong imprint of D2 (vertical shearing) and D3 (lateral shearing) on the 3D architecture of all the deposits in the studied area.

Acknowledgement

The X-mine project has received funding from the European Union's Horizon 2020 research and innovation programme under grant agreement No 730270. https://xmine.eu

References

Carlon, C., Bleeker, W., 1988: The geology and structural setting of the Håkansboda Cu-Co-As-Sb-Bi-Au deposit and associated Pb-Zn-Cu-Ag-Sb mineralisation, Bergslagen, central Sweden. Geologie en Mijnbouw 67:272–292.

Jansson, N., Sädbom, S., Allen, R., Billström, K., Spry, PG., 2018: The Lovisa stratiform Zn-Pb deposit, Bergslagen, Sweden: structure, stratigraphy, and ore genesis. Economic Geology 113:699-739.

Kampmann, T., Stephens, M., Weihed, P., 2016: 3D modelling and sheath folding at the Falun pyritic Zn-Pb-Cu-(Au-Ag) sulphide deposit and implications for exploration in a 1.9 Ga ore district, Fennoscandian Shield, Sweden. Mineralium Deposita 51:665–680.

Koark, H.J., 1960: The Geology of the Strássa, Blanka and Håkansboda Districts. A brief outline on the occasion of the XXI International Geological Congress.

Kopparberg Mineral AB, 2012: The Håkansboda project, 54 pp

Lovisagruvan AB annual report 2018. www.lovisagruvan.se

Lundström, I., 1983: Beskrivning till Berggrundskartan. Lindesberg SV: Geological Survey of Sweden, Af 126, 140 p. (in Swedish)

Magnusson, N.H., 1973: Malm i Sverige, vol 1. Mellersta och södra Sverige. Almqvist & Wiksell, Stockholm, 320 pp

Orexplore (in press). Orexplore drill core scanning technique, Orexplore White Paper. https://orexplore.com

Sahlström, F., Jonsson, E., Luth, S., Höghdahl, K., Landström, E., Sädbom, S., Lynch, E., Ghaderidosst, S., 2019: Textural evolution of the Lovisa Zn-Pb-(Ag) deposit, Bergslagen, Sweden: Insights from microscopy and 3D X-ray tomography, SGA-extended Abstracts, this volume.

Stephens, M.B., Andersson, J., 2015: Migmatization related to mafic underplating and intra- or back-arc spreading above a subduction boundary in a 2.0–1.8 Ga accretionary orogen, Sweden. Precambrian Research 264:235–257.